Atomic-resolution transmission electron microscope evidence for the mechanism by which chlorite weathers to 1:1 semi-regular chlorite-vermiculite

JILLIAN F. BANFIELD AND TAKASHI MURAKAMI

Mineralogical Institute, Graduate School of Science, University of Tokyo, Hongo, Bunkyo-ku, Tokyo 113, Japan

ABSTRACT

Atomic-resolution transmission electron microscope (TEM) images reveal that II*bb* (β = 97°) Mg,Al,Fe-chlorite from Koongarra, Australia, transforms to vermiculite via a range of intermediate chemical and structural states. Semi-quantitative analysis of contrast in atomic-resolution images of layer silicates with ~1.4 nm basal spacings indicate that the interlayers range from brucite-like to having ~0.3–0.6 interlayer cations per formula unit. Octahedral cations (predominantly Mg and Fe) tend to be removed from every second interlayer, leading to semi-regular 1:1 interstratifications of chlorite-vermiculite. Further loss of interlayer cations is accompanied by partial to complete interlayer collapse in the vacuum of the TEM. Resulting intergrowths of chlorite and semi-regular 1:1 chlorite-vermiculite retain the primary chlorite orientation, morphology, and sense of octahedral tilt in 2:1 layers. Although vermiculitization is a continuous process that occurs by a solid-state mechanism, the reaction involves important structural modifications. Atomic-resolution [010] images indicate initial loss of interlayer cations is accompanied by ~**a**/3 shifts of 2:1 layers and cations in brucite-like interlayers. Displacements of interlayer cations change the interlayer stacking from II*bb* to I*ab* and shift of the following 2:1 layer converts it from I*ab* to the I*aa*. Displacements are driven by the lower energy of *a*-type interactions when vacancies occur in sites above tetrahedral cations. Shift of a 2:1 layer alters the subsequent interlayer from II*bb* to II*ab*. Stabilization of every slightly altered second interlayer by introduction of *a*-type stacking explains development of semi-regular 1:1 chlorite-vermiculite interstratifications. Displacements occur before significant modification of interlayer electron density can be detected in high-resolution images. This observation is consistent with previously reported inhibition of layer shifts by low interlayer charge. Layer displacement may occur by an elastic process (no rupture of bonds within the 2:1 layer) at the tip of the growing vermiculite portion of the intergrowth. Removal of cations from the chlorite-vermiculite junction may be facilitated by rapid diffusion along the vacancy-rich interlayer. Mg is removed in solution, Fe is precipitated locally in aggregates of nanocrystalline Al-, Si-, and P-bearing goethite.

INTRODUCTION

Geochemical and biogeochemical cycles near the Earth's surface are greatly impacted by weathering reactions that release cations to solution and produce clay minerals. Most mineral weathering studies involve measurement of dissolution rates under conditions that preclude formation of clay minerals. In contrast, some natural weathering reactions produce abundant clays that develop topotactically on primary mineral surfaces (e.g., Eggleton 1984; Banfield and Barker 1994; Hochella and Banfield 1995). Because of structural coherence between the primary and secondary phases, polymers may be inherited by weathering products. The mechanisms of solid state or partially solid-state transformations are different from dissolution-reprecipitation and thus require different kinetic models.

The best evidence that low-temperature reactions can involve considerable structural inheritance comes from studies of naturally weathered layer silicates. Lattice-fringe TEM images indicate a layer-by-layer biotite-to-vermiculite transformation mechanism (Banfield and Eggleton 1988; Kogure and Murakami 1996) accompanied by gradual reduction in the K content of the interlayer (Kogure and Murakami 1996). Direct formation of vermiculite from biotite can also be inferred from experimental studies showing incongruent dissolution (e.g., Acker and Bricker 1992; Kalinsowski and Schweda 1996), which may be especially important at pH > 4.0 (Acker and Bricker 1992). This paper examines the detailed structural rearrangements that accompany the weathering of chlorite to vermiculite. From these data, we propose a reaction mechanism and explain the formation of semi-regular interstratified chlorite-vermiculite.

SAMPLES AND EXPERIMENTAL METHODS

Samples examined in this study are from diamond drill core from a weathered portion of the Koongarra uranium

deposit, within the Alligator River Uranium Field in Northern Australia. Geological details were summarized by Snelling (1992). Murakami et al. (1996) provide a cross section of the deposit. The silicate mineralogy of the Koongarra deposit was described by Komninou and Sverjenski (1995). Hydrothermal conversion of muscovite-$2M_1$ to a K-poor, Si-rich muscovite-$2M_1$ and formation of chlorite from solution and by replacement of altered muscovite was proposed. The quartz chlorite schist examined in this study was subjected to weathering for more than one Ma (Airey et al. 1986). Murakami et al. (1996) characterized variably weathered samples by X-ray diffraction and electron microprobe analysis (EMPA). Weathering products of Fe-rich (chamosite) and Mg-rich clinochlore) chlorite identified by X-ray diffraction (XRD) included chlorite-vermiculite intergrade (as defined by Wilson 1987), interstratified chlorite-vermiculite, vermiculite, and kaolinite.

Samples examined in this study are DDH 3-160 (37.4 m depth), DDH 3-106 (24.8 m depth), DDH 3-105 (24.5 m depth), DDH 3-103 (24.1 m depth), and DDH 4-101 (23.6 m depth). Samples range from very slightly to moderately weathered.

Approximately 30 μm thick slices were removed from petrographic thin sections and thinned to electron transparency by argon ion milling. Specimens were coated lightly with carbon and examined in a JEOL 2010 transmission electron microscope with a point resolution of 0.2 nm. Analytical electron microscope (AEM) analyses were collected with a Li-drifted Si detector and processed with a JEOL analyzer. Images were recorded on Mitsubitui film at magnifications of 150 000x to 800 000x using exposure times of ~1–6 s.

Selected areas of TEM negatives were digitized and processed to remove noise and the image of amorphous material by rotational filtering (NCEM package of Kilaas and Siddnei implemented within Digital Micrograph version 2.5, Gatan Ltd.). Details in filtered and unfiltered images were interpreted to provide atomic information by comparison with simulated images calculated using MacTempus software (Total Resolution Co.).

RESULTS

Hydrothermal mineralogy

Scherzer defocus atomic-resolution images down [100] (Fig. 1, top) clinochlore show spotty contrast associated with both octahedral sheets (small arrows in Fig. 1, top). Image simulations from chlorite with completely trioctahedral character have a continuous dark stripe over the octahedral sheets whereas images from chlorite with dioctahedral sheets have spotty contrast. Thus, contrast in Figure 1, top, indicates that both octahedral sheets in this chlorite have some dioctahedral character. AEM analyses indicate that this is mostly due to significant Al (also see EMPA analyses in Murakami et al. 1996).

The 02l and 04l rows in most [100] selected area electron diffraction patterns (SAED) patterns from unweath-
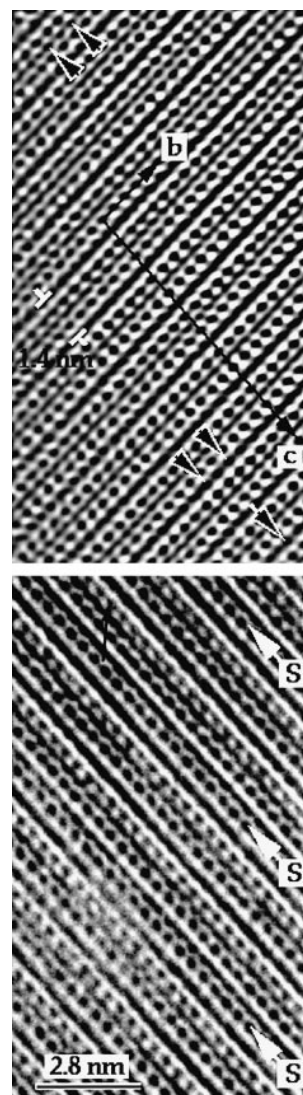

FIGURE 1. Scherzer defocus transmission electron microscope [100] images. (**top**) The brucite-like interlayer of clinochlore is imaged as a dark stripe, projected pairs of tetrahedra as black spots, and the octahedral sheet as a lighter black stripe. Some spottiness in the contrast over the octahedral sites (**arrows**) indicates dioctahedral character. Top figure has been rotationally filtered. (**botttom**) Occasional serpentine layers are indicated by arrows in the unfiltered image.

ered chlorites show maxima superimposed upon continuous streaks. However, in some regions, the stacking is regular (Fig. 1, top). The 20l reflections in SAED patterns are sharp. The abundant polytype in all samples is the IIbb polytype (β ~97°), although the Ibb polytype (β = 90°) is present also. Energy-dispersive X-ray (EDX) analyses show that chlorite Mg:Fe ratios are variable. A continuum of compositions exists between clinochlore and chamosite.

HRTEM images reveal that most chlorite crystals contain occasional serpentine layers (Fig. 1, bottom). These
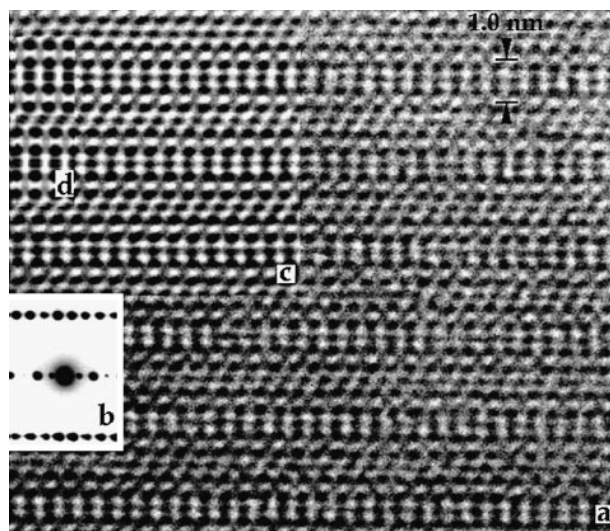
FIGURE 2. (**a**) Scherzer defocus transmission electron microscope [100] image of $2M_1$ low K, high Si muscovite; (**b**) selected-area electron diffraction pattern showing two layer period along $02l$; (**c**) rotationally filtered region of (**a**); (**d**) image simulation (defocus = −42 nm, thickness = 5 nm, Cs = 0.5 mm) assuming 0.4 K per formula unit.

typically occur as single layers, occasionally in semi-periodic intergrowths with chlorite. Small areas of dozyite (Bailey et al. 1995) were identified, and longer period arrangements (e.g., chlorite, chlorite, serpentine, as in Fig. 1, bottom) occur locally. Rarely, packets containing up to about 10 serpentine layers were detected.

Large crystals of $2M_1$ mica occur in some areas (Fig. 2). The two-layer periodicity is apparent in SAED patterns (Fig. 2b). K contents are impossible to quantify by AEM due to loss of K during analysis. This phase is characterized by high Si:Al ratios compared with ideal muscovite and 1–5% Mg and Fe. Careful examination of a series of high-resolution images recorded from a several micrometer-wide area, including the analysis region showed no chlorite or serpentine layers. Probably, Mg and Fe are incorporated in the muscovite structure.

Image simulations (Fig. 3) show that the darkest spots in Figure 2 correspond to projected pairs of tetrahedra, the dioctahedral sheet of the 2:1 layer is resolved as slightly weaker spots midway between the tetrahedra. The regular two-layer alternation of the stacking vector within the 2:1 layer (parallel and at 60° to the beam) is apparent in Figure 2. The contrast associated with interlayer K is relatively weak compared with contrast expected from ideal muscovite (see simulations in Fig. 3). Experimental images closely match calculated images at K contents of 0.3 and 0.5 per formula unit (pfu). The match between the simulation for 0.4 K pfu and experimental image is shown in Figure 2d.

Weathering of chlorite

Chlorite that is structurally and compositionally different from typical unweathered material is characterized by
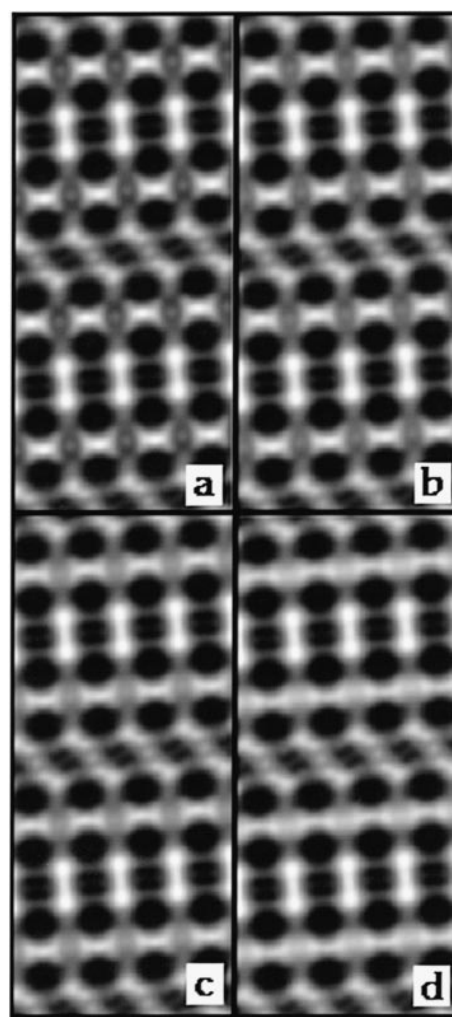
(a) K= 0.80 (b) K = 0.50
(c) K= 0.35 (d) K = 0.10

FIGURE 3. Several [100] image simulations illustrating the change in contrast in the interlayer with interlayer occupancy (defocus = −42 nm, thickness = 5 nm, Cs = 0.5 mm) for $2M_1$ muscovite with (**a**) K = 0.8 pfu, K is resolved as gray spots above the near-vertical white stripes; (**b**) K = 0.5 pfu, K can still be resolved. However, the contrast is weaker than in (**a**); (**c**) K = 0.35 pfu, K sites can just be resolved; there is still some contrast variation along the interlayer; (**d**) K = 0.1 pfu, the interlayer has almost continuous white line contrast.

streaks along the $20l$ and $40l$ rows in SAED patterns (Fig. 4). Although streaking along $02l$ and $04l$ rows in layer silicates is well understood (e.g., Bailey 1988a), streaking of $h0l$ is uncommon and has not been discussed in detail previously (e.g., Bailey 1988a, 1988b).

Figure 5a shows an atomic-resolution Scherzer defocus image recorded down [010] from a region characterized by pronounced streaking along $20l$. Contrast was manipulated in Figure 5b to emphasize discrete spots. Details in Figure 5b show that the β angle is not consistent over
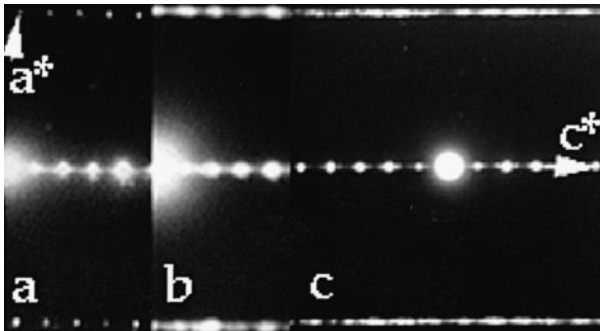
FIGURE 4. The [010] selected-area electron diffraction patterns from (**a**) fresh, and (**b**), (**c**) increasingly altered chlorite. Note the streaks along 20*l* in (**c**).

more than a few unit cells. Arrows between contrast maxima reveal displacements both of interlayer cations and 2:1 layers. The magnitude of the smallest displacement measured from the images is ~0.2 **a** (~0.106 nm).

Typically chlorite structurally modified by layer displacements is characterized by highly variable contrast associated with the brucite-like interlayer in Scherzer defocus images (e.g., Figs. 5b, 6, 7, and 8). In some areas, reduction of contrast of brucite-like interlayers correlates with layer displacement along *a** (best illustrated in Fig.
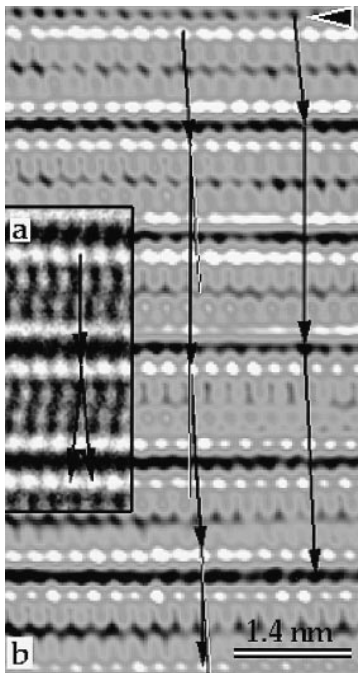

FIGURE 5. (**a**) The [010] Scherzer defocus HRTEM image of chlorite from an area characterized by a diffraction pattern similar to that in Figure 6c. The image in (**b**) was rotationally filtered and contrast enhanced to emphasize details. Note that (β) is variable (arrows) and that both interlayer cations and 2:1 layers are displaced. Displacement vectors are approximately +0.2 **a** (~0.016 nm) or approximately −0.3 **a**.
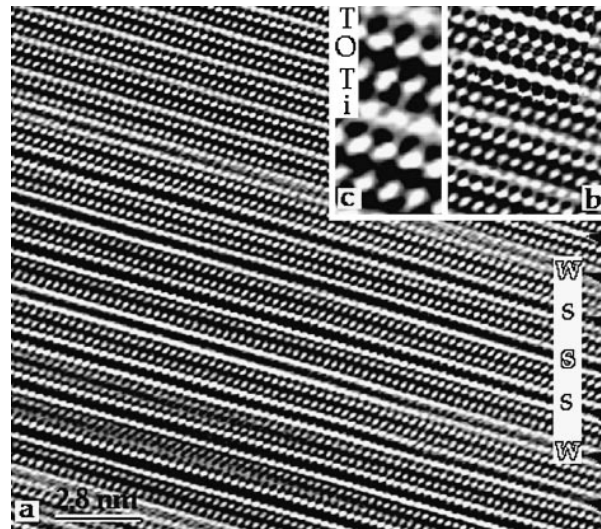

FIGURE 6. (**a**) Rotationally filtered Scherzer defocus [010] image of partially altered chlorite (**bottom**) and associated 1.0 nm phase. Arrows indicate brucite-like interlayers with variable S (strong) vs. W (weak) contrast. To our knowledge, [010] zone axis atomic-resolution images of layer silicates have not been previously published. Consequently, the area in (**b**) is enlarged (with superimposed image simulation) and in (**c**) is labeled to show the correspondence between tetrahedral cations (spots), the octahedral sheet (spotty stripes) and the interlayer. Simulations and details for chlorite are shown elsewhere.

7) and superposition of tetrahedral sites across low-contrast interlayers (Fig. 7b).

Lower contrast interlayers tend to develop adjacent to darker contrast interlayers and in some areas this leads to a semi-regular alternation (see Fig. 7). Note that displacements (arrows in Fig. 7) correlate with lower contrast interlayers. In some interlayers, octahedral sites (projected M3 and M4 sites) are clearly resolved as spots (Fig. 8). Image simulations for clinochlore (Fig. 9) indicate that contrast changes due to interlayer occupancy are not apparent until the M3 and M4 sites are about half occupied. Distinct spots occur when the interlayer site occupancy approaches 0.2 (0.6 cations pfu; however, simulations with interlayer occupancies of 0.1 are not substantially different). On the basis of visual comparison with experimental images, the interlayer in partly weathered chlorite (that retains the 1.4 nm basal spacing in the vacuum) may range from brucite-like (as in ideal chlorite) to near vermiculite-like.

Interstratifications with interlayers that are more brucite-like alternate in a semi-periodic fashion with layers characterized by 1.0 nm basal spacings (note the obvious ~2.4 nm separation of higher contrast interlayers in Fig. 10). The spacings between these interlayers is commonly variable. In Figure 10, for example, more brucite-like interlayers are separated by ~2.37 to 2.63 nm. The largest spacings are observed where low-contrast relicts remain in the more vermiculite-like interlayer (see arrow in Fig. 10).
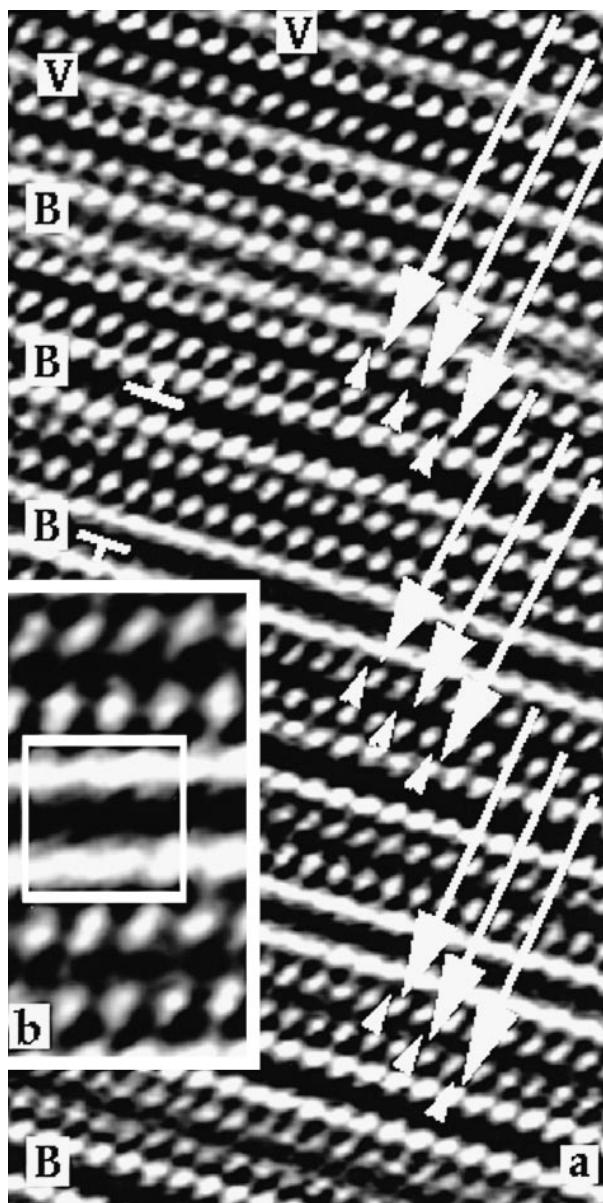
FIGURE 8. Rotationally filtered Scherzer defocus [010] image of chlorite characterized by highly variable contrast over the brucite-like interlayers (B). Especially low contrast interlayers are indicated by arrows. Note that these have spotty contrast in some areas (double arrows).

FIGURE 7. (**a**) Rotationally filtered Scherzer defocus [010] image of chlorite from an area characterized by intense streaking along 20*l*. Vermiculite interlayers are indicated by (V) and brucite-like interlayers with a separation of 1.4 nm are indicated by (B). Arrows indicate displacements of the entire 2:1 layer. Note that displacements occur every second chlorite unit, correlating with low contrast in the preceding brucite-like interlayer. (**b**) Enlargement of (**a**) showing that dark contrast spots (associated with tetrahedral sites) superimpose over an altered interlayer, unlike in I*bb* or II*bb* chlorite.

EDX analyses of regions consisting of mixtures of 1.4 and 1.0 nm phases show similar Al:Si ratios but lower Mg and Fe contents than chlorite. XRD analyses of clays from DDH 3-105 indicated exchange behavior consistent with a vermiculite-like phase but thermal behavior resembling chlorite (Murakami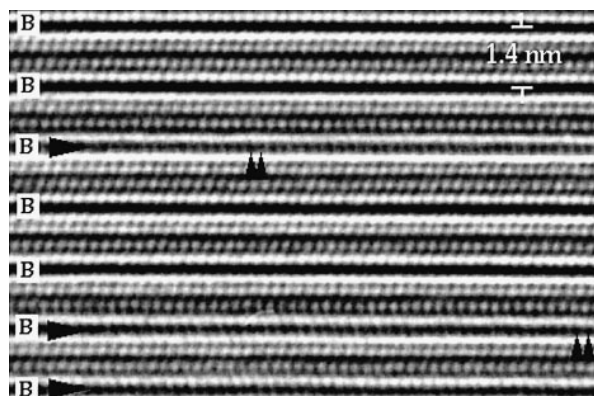 et al. 1996). This behavior is consistent with layer charge intermediate between chlorite and vermiculite. Units with modified contrast but 1.4 nm spacings are interpreted as chlorite-vermiculite intergrade and those with ~1.0 nm basal spacings (Figs. 10, 11, and 12) are probably vermiculite.

Figure 11 is Scherzer defocus [010] zone axis image showing interlayers with more brucite-like contrast (site occupancies probably > 0.5) every fourth interlayer. On the left and right sides, the two interlayers bracketed by brucite-like interlayers have highly modified contrast. These layers probably have occupancies approaching, but not equal to, those of vermiculite (see Fig. 9). In the center of Figure 11, the brucite-like interlayers enclose layers with ~1.0 nm basal spacings. The interlayer occupancy of this material is too low to prevent collapse in the TEM vacuum. Thus, the layer spacings in Figures 10 and 11 are artifacts of differential collapse, reflecting subtle differences in interlayer occupancies. The sequence in Figure 11 approaches chlorite-vermiculite-vermiculite (but is periodic only over the area shown).

In DDH 3-103 and DDH 4-10, layer silicates are a fine-scale intergrowth of chlorite, semi-regular 1:1 chlorite-vermiculite interstratifications, and minor vermiculite (Fig. 12, top). SAED patterns show broad (00*l*) reflections with diffuse maxima corresponding to 1.2, 0.8, and 0.6-0.7 nm (Fig. 12, bottom). These regions preserve the (often bent) crystal shapes of primary chlorite as well as the primary grain orientations, which in some cases involve intergrowths of packets of chlorite with [010] parallel to [100].

Despite complications due to the variable Fe:Mg ratio of primary chlorite, AEM analyses suggest alteration is associated with significant loss of Fe and Mg, resulting in aluminous vermiculite. Packets of 1.0 nm material coexist with interstratified chlorite and chlorite-vermiculite in some regions of more altered samples. These occasionally contain uncollapsed layers with more brucite-like character (Fig. 13). The β angle for the 1.0 nm phase is
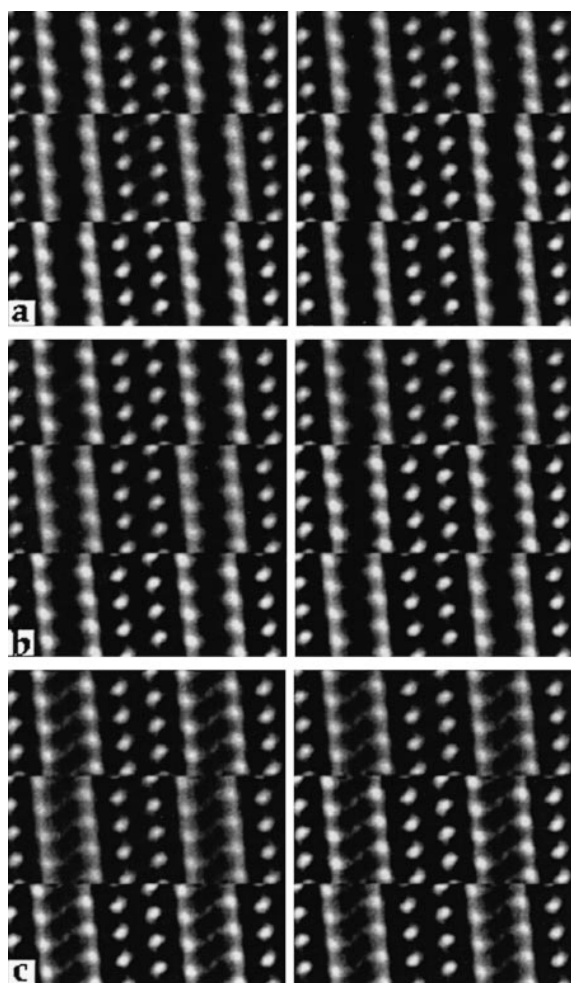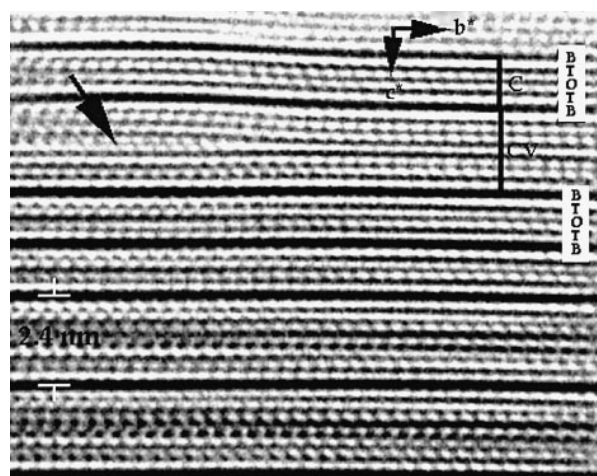
FIGURE 10. Rotationally filtered Scherzer defocus [100] image of interstratified chlorite-like and vermiculite-like material. Note the three chlorite-vermiculite units (~2.4 nm separation of more brucite-like interlayers). The arrow indicates a vermiculite-like interlayer that contains a small area of low contrast material that is associated with increase in the separation of enclosing more brucite-like interlayers from ~2.37 to 2.63 nm.
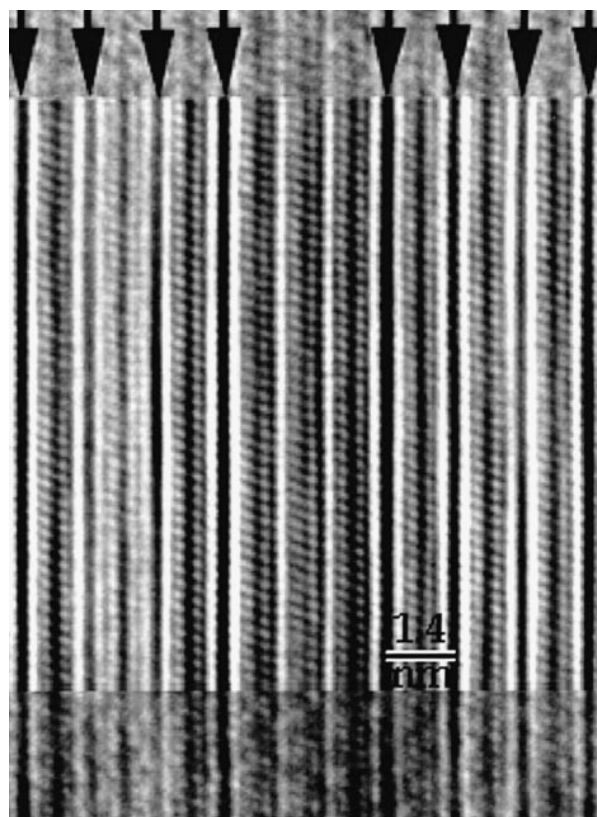
FIGURE 9. Simulations of high-resolution images of chlorite (II*bb* structure of Rule and Bailey 1987) calculated using parameters for a JEOL 2010 HRTEM with Cs = 0.5 mm at close to Scherzer defocus. The left column shows results for a sample 5 nm thick and the right column for a sample 7 nm thick. The defocuses for the top, middle, and bottom rows in each group are −40, −42, and −44 nm (**a**) M3 and M4 sites fully occupied, (**b**) each M3 and M4 site is half occupied (1.5 interlayer cations pfu), (**c**) each M3 and M4 site 20% occupied (0.6 interlayer cations pfu).

FIGURE 11. Rotationally filtered Scherzer defocus [010] image of interstratified chlorite-like and vermiculite-like layers superimposed over the unfiltered image. Arrows indicate the positions of interlayers associated with layers with 1.4 nm basal spacings. Such sequences do not persist over large distances.

close to 97° (Fig. 13 inset; but 90° in some cases). The polytype for the vermiculite-like phase was not uniquely determined, but SAED data are consistent with I*aa,* which is the common structure identified in XRD studies of vermiculite (de la Calle and Suquet 1987).

Iron precipitation results in local concentrations of semi-oriented aggregates of goethite nanocrystals between packets of altered layer silicates. These have an approximately topotactic orientation ([001] goethite parallel to [010] chlorite-vermiculite and $b*$ goethite parallel to $a*$ chlorite-vermiculite), implying Fe-dominated octahedral strips in goethite are parallel to octahedral sheets
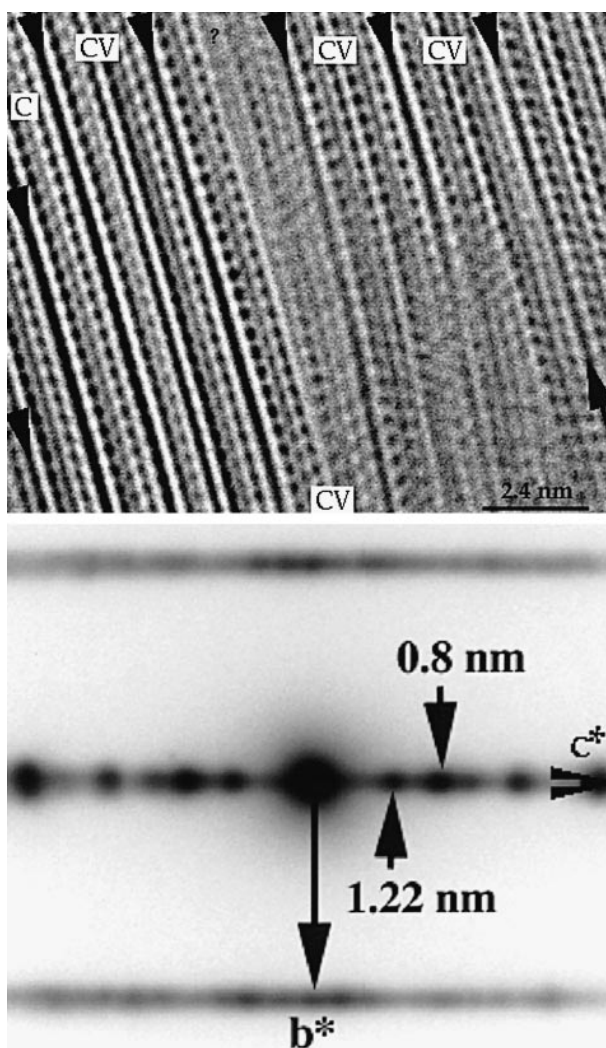
FIGURE 12. (**top**) Scherzer defocus [100] image of typical interstratified chlorite-vermiculite (CV) and chlorite-like (C) material in the most weathered samples examined. Low contrast, wedge-shaped areas (e.g., ?) may be space produced by collapse across vermiculite-like interlayers in the vacuum. (**bottom**) SAED pattern for an area of material including that in top figure. Note that fuzzy spots along 00*l* at 1.22 and 0.8 nm are expected diffraction maxima associated with mixed layer chlorite-dioctahedral vermiculite (**bottom**).

FIGURE 13. Rotationally filtered Scherzer defocus [010] image of the 1.0 nm phase containing isolated interlayers with some brucite-like character. (Inset in upper right corner) Fourier transform of (**a**) showing discrete 20*l* reflections and β ~97°.

in associated layer silicate. Topotactic packets of kaolinite are also present in some regions.

DISCUSSION

Mineralogy of the least-altered samples

The mineralogy of these samples is similar to that reported by Komninou and Sverjensky (1995). The Si-rich muscovite-$2M_1$ was shown to be K-deficient relative to ideal muscovite (~0.4 K per formula unit). This composition is similar to that proposed by Komninou and Sverjensky (1995). Probably this illite-like phase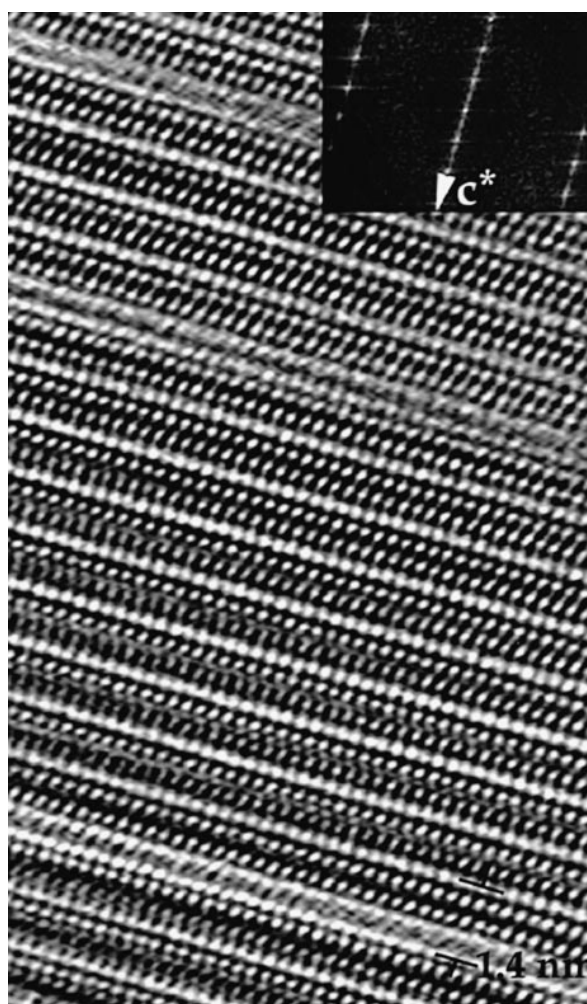 was formed by a continuous process that did not require dissolution and reprecipitation of the basic structure. Illitization may have occurred either during weathering or a low-temperature hydrothermal event.

Weathering

Structural and chemical data are interpreted to indicate a continuous range of site occupancies in the brucite-like interlayer of weathered chlorite. In addition, the sense of shift in the 2:1 layer is inherited by the vermiculite-like product. Thus, we propose that chlorite was vermiculitized by a continuous, solid-state mechanism. The lower activation energy for direct structural modification compared with bulk dissolution and recrystallization can be explained based on the high degree of structural correspondence between chlorite and vermiculite (the 2:1 layer is almost identical).

The result that natural chlorite weathering is incongruent (at least under some conditions) differs from conclu-

sions reached by many previous workers. Nagy (1995) noted that although most laboratory studies report non-stoichiometric dissolution early in experiments, dissolution is congruent in the later stages. The more recent results of Malmstrom et al. (1996) for chlorite dissolution at near-neutral pH are similar to those reviewed by Nagy (1995).

In contrast to dissolution studies where all constituents are released into solution, the fate of constituents initially present in the chlorite examined here is highly variable. Si and Al are retained in the intergrown chlorite- and vermiculite-like material. A significant fraction of the Mg and Fe are released, Mg to solution and Fe to form secondary Fe-oxides. These results for chlorite are analogous to those for naturally weathered biotite (Banfield and Eggleton 1988; Kogure and Murakami 1996) and from some experimental dissolution studies (Acker and Bricker 1992). The complexity evident in some kinetic studies of layer silicate dissolution (see discussion in Kalinowski and Schweda 1996) is understandable in view of these data.

Despite the continuous nature of compositional changes, results show that all structural characteristics of chlorite are not inherited. An early step in the vermiculitization reaction involves shifts of some 2:1 layers with respect to adjacent layers. Where these shifts occur frequently but nonperiodically, there is no fixed value of β, resulting in streaking (or spottiness) along 20*l*.

Direct measurements from atomic-resolution images show that the smallest shift between 2:1 layers is ~0.2 **a**, equivalent to a shift of ~0.3 **a** in the opposite direction. The vector 0.3**a** is close to the **a**/3 vector that separates a from b positions in the interlayer. Figure 14 shows the consequences of a series of **a**/3 displacements of interlayer cations and a 2:1 layer. The gray line connects tetrahedra (gray circles) in the lower 2:1 layer, and the solid line connects tetrahedra in the 2:1 layer above the interlayer of II*bb* chlorite. If the interlayer cations (circles with +) are displaced downward by **a**/3 (arrows), M3 sites superimpose directly onto tetrahedral sites in the 2:1 layer below (Fig. 14a). Note that this displacement alters the interlayer octahedral tilt so that the chlorite unit, consisting of this interlayer and the underlying 2:1 layer, is now I*ab* (interlayer hydroxyls remain fixed).

If the 2:1 layer above (gray circles linked by solid black lines) relocates by an upward shift of **a**/3 (Fig. 14b), the structure in this region becomes I*aa,* as expected for vermiculite. Note that pseudohexagonal cavities oppose each other, so the upper tetrahedral cations project directly onto the interlayer cations and the tetrahedral cations below (as in Fig. 7b).

A predominant product of chlorite weathering in the samples described here is a regular 1:1 interstratification of chlorite and vermiculite. Johnson (1964) also identified this as the product of chlorite weathering and suggested it formed from a two-layer chlorite polytype by selective alteration of one of the two interlayers. However, no evidence exists for a two-layer polytype in chlorite studied
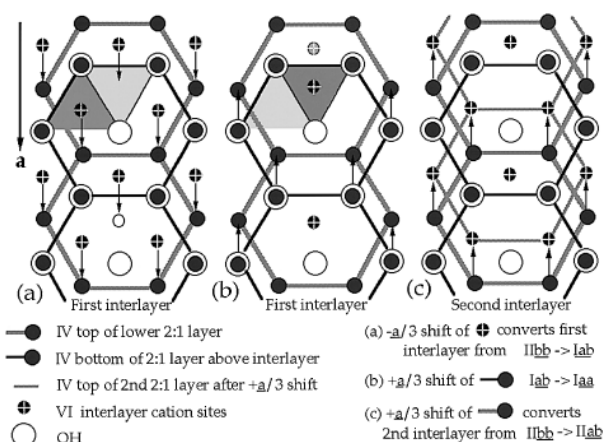

FIGURE 14. Schematic diagram illustrating cation sites projected onto (001). (**a**) conversion of an interlayer in II*bb* chlorite to I*ab* by displacement of interlayer cations by −**a**/3. As a consequence, interlayer cations superimpose on tetrahedral sites in the 2:1 layer below. (**b**) Illustrates that this interlayer is converted by I*aa* if the 2:1 layer above shifts by +**a**/3. The effect of this 2:1 layer shift on the next interlayer (above) is shown in (**c**). Conversion of the second interlayer to II*ab* changes its stability. This reveals how changes needed to form one vermiculite-like interlayer affect the stability of the next, leading to semi-regular 1:1 interstratifications.

here (or in similar weathered chlorite examined by Churchman 1980).

Formation of 1:1 chlorite-vermiculite must involve changes in stability of every second brucite-like interlayer as a consequence of modification of the first. Figure 14c shows that the ~**a**/3 displacement of TOT layers observed in [010] images (transforms the first interlayer to I*aa*) also changes the subsequent interlayer, converting it from II*bb* to II*ab*. These displacements are summarized in Figure 15 (similar displacements are required to create *aa* character in the interlayer of I*bb* chlorite).

The apparent stability of the alternate interlayers (II*ab*) suggests these have lower interlayer site occupancies than original II*bb* brucite-like interlayers. However TEM observations of semi-regular 1:1 interstratifications of vermiculite and more chlorite-like layers suggest that further cation loss from these more brucite-like interlayers is arrested. This may result from the introduction of *a*-type character, which reduces the energy of the partly vermiculitized interlayer region (i.e., II*bb* → II*ab*), and thus reduces the driving force for further displacements. Consequently, interlayer shift is the vehicle by which modification of one layer affects the reactivity of the next. In conclusion, semi-regular chlorite-vermiculite formation is partly a consequence of the kinetic controls, which favor direct structural transformation over dissolution-reprecipitation. It is also partly the result of an energy minima resulting from increased stability of alternate interlayers due to reduction in repulsion between interlayer cations and cations in tetrahedral sites.

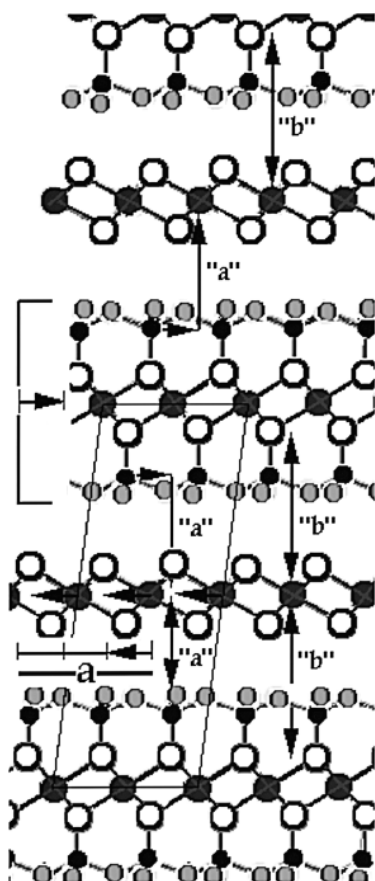Shifts of entire 2:1 layers during a weathering reaction

FIGURE 15. Diagram illustrating changes in II*bb* chlorite as shown in Figure 7 (viewed down [010]). Horizontal arrows indicate shifts and vertical arrows indicate cation projections (*a* and *b* type).

are perhaps surprising, given that the justification for solid state transformation is minimization of structural rearrangement. However, analogous layer shifts take place during (diagnostic) vermiculite cation exchange reactions. For example, de la Calle and Suquet (1987) note that cation exchange in vermiculite is accompanied by changes in the relative positions of the 2:1 layers. Although these cation exchange reactions differ in detail, such observations show that 2:1 layer displacements can take place in response to changes in the interlayer easily and at low temperature.

Similar layer shifts accompany the solid-state serpentine-to-chlorite reaction in metamorphic rocks (Banfield and Bailey 1996). Presumably these shifts are driven by the greater stability of type *b* vs. type *a* interactions between octahedral interlayer cations and cations in the tetrahedral and octahedral sites in the 2:1 layer of trioctahedral chlorite. Banfield and Bailey (1996) suggested that the shift of the 2:1 layer occurs sequentially as the new 2:1 layer forms, with the displacement accommodated at the junction by elongation of tetrahedral-O bonds. In this case, and in the vermiculitization of chlorite, changes in

the relative positions of 2:1 layers occur elastically. We predict that other solid-state layer silicate alteration reactions (e.g., muscovite or biotite-1*M* ↔ chlorite-II*bb*) should involve analogous displacements (and polytypic changes) to those documented here.

The relative stability of a-type interactions in the I*aa* structure of vermiculite was attributed to vacancies in energetically unfavorable sites directly above tetrahedral cations (Bailey 1988b). Conversely, high site occupancies in the brucite-like interlayer of chlorite favor *b*-type stacking with sites that avoid superposition over tetrahedral cations. As chlorite vermiculitization increases the number of vacancies on interlayer sites, the stability of *b*- vs. *a*-type stacking is reversed. In the chlorite-to-vermiculite reaction, these cationic interactions are clearly sufficiently important to trigger displacement of interlayer cations and the associated 2:1 layers.

Cation exchange studies of vermiculite show that layer displacements are inhibited where interlayer charge is low (de la Calle and Suquet 1988). This is attributed to reduction in cationic repulsions originating between the 2:1 layer and interlayer. This is consistent with the findings of this study. These findings show that layer displacement occurs early in the chlorite-to-vermiculite weathering reaction when interlayer occupancies are still close to (but lower than) those of chlorite.

Our results show that Fe was transported many micrometers from reaction sites. We do not know the pH or redox state of solutions at grain boundaries and in narrow fluid conduits at the time of reaction. However, the solutions were probably chemically and physically distinct from bulk meteoric H_2O. Presumably, Fe was moved from reaction sites inside crystals by interlayer diffusion, transported by solution as Fe^{2+} to more oxidized regions, and reprecipitated. This resulted in formation of aggregates of nanocrystals of goethite, which nucleated and grew topotactically on layer silicate surfaces.

Although most studies concur that vermiculitization is associated with loss of Mg and Fe, the role of Fe oxidation is unclear (Ross and Kodama 1976; Proust et al. 1986). If iron is removed from chlorite as Fe^{2+}, as suggested above, charge imbalance due to oxidation does not trigger loss of interlayer cations and other changes associated with vermiculitization.

We cannot unequivocally establish the role of Fe oxidation in promoting vermiculitization. However, it is useful to examine what other charge balance changes could promote loss of interlayer cations. A fundamental difference between chlorite and vermiculite is the presence of H_2O molecules in place of hydroxyl groups surrounding interlayer cations. Our data imply a range of interlayer compositions exist involving any mixture of $M_{3-x}(OH)_6$ and $M_{3-y} \cdot n\ H_2O$ (where x and y indicate dioctahedral character in the brucite-like and vermiculite interlayer, respectively, and n is the number of H_2O molecules). Thus, an increase in a_{H^+} may result in sequential protonation of hydroxyls in the chlorite interlayer, with charge balance maintained by loss of interlayer cations, not unlike ex-

changes proposed to operate in other mineral weathering reactions (e.g., $Na^+ \leftrightarrow H^+$ and $Ca^+ \leftrightarrow 2H^+$ in weathering of feldspars). A strong pH dependence of alteration rates [analogous to that reported by Kalinowski and Schweda (1996) for trioctahedral micas] would support this suggestion.

Formation of vermiculite, kaolinite, and goethite

Some samples contain highly altered regions of vermiculite, kaolinite, and goethite. Loss of Mg and Fe from octahedral sites in chlorite results in vermiculite layers with considerable dioctahedral character. Although the original distribution of Al between octahedral sites in the 2:1 layer and brucite-like interlayer is not known, [100] zone axis images suggest sites in both octahedral sheets have limited dioctahedral character. If the resulting vermiculite has Mg in the interlayer, as suggested by Murakami et al. (1996), exchange of Al and Mg between the 2:1 layer and interlayer may occur. Chlorite-vermiculite may be converted to vermiculite by removal of cations from remaining brucite-like interlayers (with some structural rearrangement). Alternatively, vermiculite formation from chlorite-vermiculite may involve dissolution-reprecipitation, as is probably the case for formation of kaolinite.

REFERENCES CITED

Acker, J.G. and Bricker, O.P. (1992) The influence of pH on biotite dissolution and alteration kinetics at low temperature. Geochimica et Cosmochimica Acta, 56, 3073–3092.

Airey, P.L., Golian, C., and Lever, D.A. (1986) An approach to the mathematical modeling of the uranium series redistribution within ore bodies: Topical report AAEC/C49, 106 p. Australian Nuclear Science and Technology Organization, Sydney.

Bailey, S.W. (1988a) X-ray diffraction identification of the polytypes of mica, serpentine, and chlorite. Clays and Clay Minerals, 36, 193–213.

———(1988b) Chlorites: Structures and crystal chemistry. In Mineralogical Society of America Reviews in Mineralogy, 19, 347–398.

Bailey, S.W., Banfield, J.F., Barker, W.W., and Katchen, G. (1995) Dozyite, a 1:1 regular interstratification of serpentine and chlorite. American Mineralogist, 80, 65–77.

Banfield, J.F. and Bailey, S.W. (1996) Formation of regularly interstratified serpentine-chlorite minerals by tetrahedral inversion in long-period serpentine polytypes. American Mineralogist, 81, 79–91.

Banfield, J.F. and Barker, W.W. (1994) Direct observation of reactant-product interfaces formed in natural weathering of exsolved, defective amphibole to smectite: Evidence for episodic, isovolumetric reactions involving structural inheritance. Geochimica et Cosmochimica Acta, 48, 1419–1429.

Banfield, J.F. and Eggleton, R.A. (1988) Transmission electron microscope study of biotite weathering. Clays and Clay Minerals, 36, 47–60.

Churchman, G.J. (1980) Clay minerals formed from micas and chlorites in some New Zealand soils. Clay Minerals, 15, 59–76.

de la Calle, C. and Suquet, H. (1987) Vermiculite. In Mineralogical Society of America Reviews in Mineralogy, 19, 455–492.

Eggleton, R.A. (1984) Formation of iddingsite rims on olivine: A transmission electron microscope study. Clays and Clay Minerals, 32, 1–11.

Hochella, M.F. and Banfield, J.F. (1995) Chemical weathering of silicates in nature: A microscopic perspective with theoretical considerations. In Mineralogical Society of America Reviews in Mineralogy, 31, 353–401.

Johnson, C.J. (1964) Occurrence of regularly interstratified chlorite-vermiculite as a weathering product of chlorite in a soil. American Mineralogist, 49, 556–572.

Kalinowski, B.E. and Schweda, P. (1996) Kinetics of muscovite, phlogopite, and biotite dissolution and alteration at pH 1-4, room temperature. Geochimica et Cosmochimica Acta, 60, 367–385.

Kogure, T. and Murakami, T. (1996) Direct identification of biotite/vermiculite layers in hydrobiotite using high-resolution TEM. Mineralogical Journal, 18, 131–137.

Komninou, A. and Sverjenski, D.A. (1995) Pre-ore hydrothermal alteration in an unconformity-type uranium deposit. Contributions to Mineralogy and Petrology, 121, 99–114.

Malmstrom, M., Banwart, S., Lewenhagen, J., Duro, L., and Bruno, J. (1996) The dissolution of biotite and chlorite at 25 degrees C in the near-neutral pH region. Journal of Contaminant Hydrology, 21, 201–213.

Murakami, T., Isobe, H., Sato, T., and Ohnuki, T. (1996) Weathering of chlorite in a quartz-chlorite schist: 1. Mineralogical and chemical changes. Clays and Clay Minerals, 44, 244–256.

Nagy, K.L. (1995) Dissolution and precipitation kinetics of sheet silicates. In Mineralogical Society of America Reviews in Mineralogy, 31, 173–215.

Proust, D., Eymery, J-P., and Beaufort, D. (1986) Supergene vermiculitization of a magnesian chlorite: iron and magnesium removal processes. Clays and Clay Minerals, 34, 572–580.

Ross, G.J. and Kodama, H. (1976) Experimental alteration of chlorite into a regularly interstratified chlorite-vermiculite by chemical oxidation. Clays and Clay Minerals, 24, 183–190.

Rule, A.C. and Bailey, S.W. (1987) Refinement of the crystal structure of a monoclinic ferroan clinochlore. Clays and Clay Minerals, 35, 129–138.

Snelling, A.A. (1992) Geologic setting, Alligator Rivers Analogue Project Final Report. Vol. 2. Australian Nuclear Science and Technology Organization, Sydney.

Wilson, M.J. (1987) X-ray powder diffraction methods. In M.J. Wilson, Ed., A handbook of determinative methods in clay mineralogy, p. 26–98. Chapman and Hall, New York.